Modelling the vibration response of a laminated beam based on equivalent material properties

Xuhao Du (1), Lingzhi Li (2), Andrew Guzzomi (1), Ming Jin (2) and Jie Pan (1)

(1) Department of Mechanical Engineering, The University of Western Australia, Perth, Australia
(2) College of Biomedical Engineering and Instrument Science, Zhejiang University, Hangzhou, China

ABSTRACT

Correct and efficient model of the dynamics of the laminated core structure is essential for the design of quiet power transformers. In this paper, the viscosity and friction between two adjacent laminas of a laminated beam were included in the derivation of the equivalent bending stiffness of the beam subject to transverse vibration. As a result, the equivalent stiffness and loss factor of the beam were obtained as functions of the lamina number and relative deformation ratio due to the friction factor between the layers. The equivalent material properties were then used to determine the frequency response functions of laminated beams using the finite element method. The comparison between the simulated and measured frequency response functions of laminated beams showed good agreement.

1 INTRODUCTION

Transformer noise is becoming a pressing environmental issue and driving manufacturers to develop quiet transformers. The design of quiet transformers relies on accurate modelling of the transformer core vibration (Girgis et al. 2008). However, there is still a lack of transformer core models, which can correctly predict the core vibration based on electric input. The main obstacle is the lack of a clear understanding of the dynamic properties of the transformer core, consisting of laminated structures with incomplete bonded and glued conditions. The finite element method (FEM) is a common tool for modelling such laminated systems. However, modelling hundreds of the laminas within one core will consume enormous computation resources. Hence, an equivalent material properties is a preference (Wang et al. 2011) in describing the vibration of the laminated structure in terms of that of a solid structure with equivalent material properties. Due to the laminated configuration, small shear stress between the lamina causes it to exhibit orthotropic properties of structural stiffness, which reduces the bending stiffness in the direction perpendicular to the lamination and increase the damping ratio of the whole core structure significantly. Several models were developed to obtain equivalent properties (Pirnat *et al*. (2013) and (Du *et al.* 2017). The former used two contact parameters to define the elastic and dissipative forces and optimised them via FEM and the experimental results. Good agreement (13% error) was obtained for the natural frequencies under different stacking structures. However merely modelling the natural frequencies correctly is not adequate for vibration prediction and noise performance because the forced vibration of a structure is also dependent on the mode shapes and damping ratios. Du *et al.* (2017) developed an empirical model based on the experimental result. Good agreement was obtained on both the natural frequencies and damping ratios while the model provides little physical understanding of the system. Besides, the damping model was developed between two laminas from a bolted friction two-beam-column system (Bournine *et al.* 2011). They started modelling the damping by considering the work done by friction and potential energy of bending. A very close agreement was obtained between experiment and model. However, their study was limited to two laminas. Transformer cores are made of multi-lamina structural components.

In this paper, the frequency response function (FRF) of a multi-lamina structure was modelled by considering the relative displacement between the adjacent laminas generated by incomplete bonding. Both the equivalent stiffness and loss factor were calculated as a function of lamina numbers and relative strain, which were modelled from a set of experimental results. The remainder of the paper is constructed as the follows: the second section presents the derivation of the analytical model including the equivalent stiffness and structure loss factor. The third section gives the experimental results including the parameters optimisation and their application to FEM. The results from FEM with the estimated equivalent stiffness and loss factor are compared with the experimental result.

2 ANALYTICAL MODEL

To assemble the transformer core, each lamina is insulated on all external surface and then stack as a laminated beam by the clamp or cable tie. Then, all the external surface of the whole laminated bar is painted. Due to the capillary effect, the adhesive penetrates into the space between laminas. The contact between adjacent laminas and resulting bond are therefore not uniform. This complicates modelling. To simplify the modelling, an assumption of uniform glue adhesive is made and uniform stiffness and friction between the laminas are described by spring-damper elements, as shown in Fig. 1. The force introduced by the spring-damper element is proportional to the relative displacement and energy is dissipated during the beam deflection. The spring-damper model is a non-linear system and will be derived in the following sections.

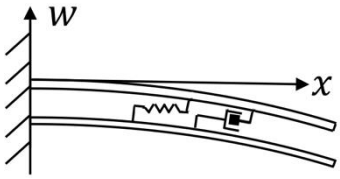

Figure 1: Spring-damper model between adjacent laminas

2.1 Equivalent Stiffness

Small deflection of the laminated beam is assumed to ensure the thickness of each lamina remains constant and Poisson effects ignored. Subsequently, three conditions of relative slip between adjacent lamina surfaces under various bonded condition are presented in Fig. 2, where (a) represents a fully bonded or solid beam, (b) is with some friction such that slip occurs between laminas and (c) is entirely frictionless. For (b) to remain valid in addition to the small transverse displacement, it assumed that the coefficient of friction is sufficient to transmit the required shear at each interface without further slip.

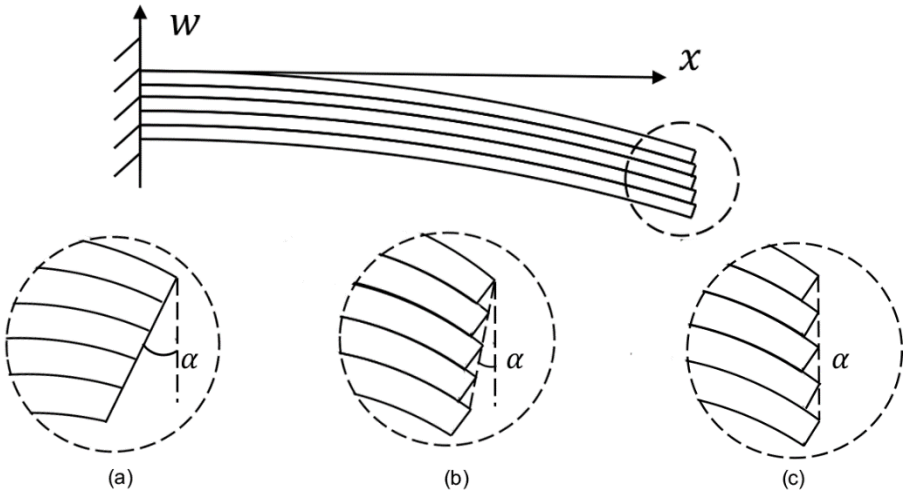

Figure 2: The edge deformations at the free end of the cantilever beam with their angle notation

For the case presented in Fig. 2(a), which is a solid beam with the same thickness, the free end is described by a straight and flat edge surface, implying that the strain of the lower surface of i^{th} lamina is equal to the strain of the upper surface of i^{th} -1 lamina. For the frictionless case as presented in Fig. 2(c), no shear force is transmitted between adjacent laminas, which means stiffness of the spring in Fig. 1 is equal to 0. For this case, the edge of the free end is jagged, and the upper corners at the free end of all laminas lie on a vertical line and in parallel with the supporting boundary. Additionally, the strain of all the upper and lower surface are the same respectively. The condition shown in Fig. 2(b) is the intermediate case. Even though the bond condition is different based on the glue condition, it is reasonable to assume that all upper and lower corners lie on the same lines, although they may not be in parallel with the supporting boundary. Fig. 3 shows an element of the i^{th} lamina under bending

condition. The upper and lower lengths of the element and the relationship of the element with respect to the neutral axis and the centre of the curvature are also illustrated in Fig. 3.

Defining strains of the upper and lower surfaces of the element of the *i*th lamina as ε_u^i and ε_l^i. The lengths of the upper and lower surfaces are expressed respectively as:

$$L_u^i = (1+\varepsilon_u^i)L_n \tag{1}$$

$$L_l^i = (1+\varepsilon_l^i)L_n \tag{2}$$

where L_n is the length of the element in the neutral axis. Since the corners of the element lie on a straight line, the strain difference between adjacent laminas should be the same for all laminas, and the strain difference between contacting upper and lower surfaces of adjacent laminas are the same as well. Therefore following two strain differences:

$$\delta_I \equiv \varepsilon_u^i - \varepsilon_l^i \tag{3}$$

$$\delta_E \equiv \varepsilon_l^i - \varepsilon_u^{i-1} \tag{4}$$

are defined to represent the internal and the external strain differences respectively. There are *N* laminas in Fig. 3. The bottom lamina is noted as the *1*st lamina and the top one is the Nth lamina. Since the beam is symmetrical about its neutral axis, without losing generality, *N* is assumed to be an odd number and thus the central geometric plane of the middle lamina is the neutral axis. As a result, the strains of the upper and lower surfaces of the *i*th lamina element can be expressed in terms of δ_I and δ_E as:

$$\varepsilon_u^i = (i-\frac{N}{2})\delta_I + (i-\frac{N+1}{2})\delta_E \tag{5}$$

$$\varepsilon_l^i = (i-\frac{N}{2}-1)\delta_I + (i-\frac{N+1}{2})\delta_E \tag{6}$$

The bending moment associated with the bending of the element can be calculated.

$$M_x = \int_{-\frac{Nl}{2}}^{\frac{Nl}{2}} r dF_x = Eb\sum_{i=1}^{N}\int_{d_i}^{d_i+l}\frac{r^2}{R_i}dr \tag{7}$$

where the differential force on the *i*th lamina of the element is calculated by $dF_x^i = \frac{rb}{R_i}Edr$ and R_i is the radius of the curvature of the *i*th lamina. In Eq. (7) l is the thickness of a single lamina and di is distance from neutral axis

to lower surface of i^{th} lamina, and b is the width of the beam. r is the distance to the neutral axis, E is Young's modulus. From the geometry shown in Fig. 3, the d_i and R_i can be expressed by their strains ε_u^i, ε_l^i.

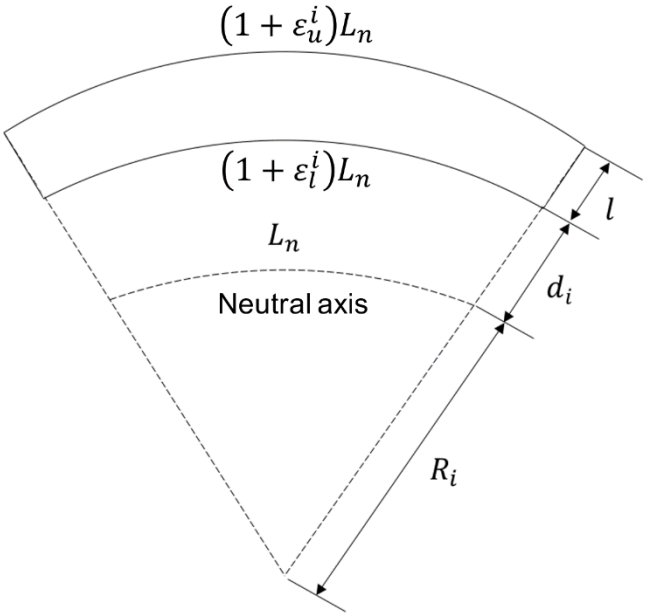

Figure 3: The configuration between the bending radius, neutral axis and the i^{th} lamina

In Fig. 3, the upper and lower surfaces are the integration boundaries as d_i and $d_i + l$. The relationship among each length can be concluded in Eq. (9).

$$\frac{R_i + d_i + l}{(1+\varepsilon_u^i)L_n} = \frac{R_i + d_i}{(1+\varepsilon_l^i)L_n} = \frac{R_i}{L_n} \tag{8}$$

Simplifying Eq. (9), the bending radius and the integration boundaries can be obtained as:

$$R_i = \frac{l}{\varepsilon_u^i - \varepsilon_l^i} = \frac{l}{\delta_I} \tag{9}$$

$$d_i = \varepsilon_l^i R_i = \varepsilon_l^i \frac{l}{\delta_I} \tag{10}$$

As a result, the bending moment can be expressed as a function of the strain difference ratio $\zeta \equiv \frac{\delta_E}{\delta_I}$ and

$$M_x = \frac{Eb\delta_I}{3l}\sum_{i=1}^{N}\int_{\varepsilon_l^i\frac{l}{\delta_I}}^{\varepsilon_u^i\frac{l}{\delta_I}} dr^3$$
$$= \frac{Ebl^2}{3\delta_I^2}\sum_{i=1}^{N}[((i-\frac{N}{2})\delta_I + (i-\frac{N+1}{2})\delta_E)^3 - ((i-\frac{N}{2}-1)\delta_I + (i-\frac{N+1}{2})\delta_E)^3] \quad (11)$$
$$= \frac{Ebl^2\delta_I}{12}[(\zeta+1)^2N^3 - (\zeta^2+2\zeta)N]$$

Considering the fully bonded and frictionless conditions, the strain difference ratios ζ equal to 0 and -1, respectively. Thus the corresponding bending moments are:

$$M_{x,\,fully\ bounded} = \frac{Ebl^2\delta_I}{12}N^3 \quad (12)$$

$$M_{x,\,frictionless} = \frac{Ebl^2\delta_I}{12}N \quad (13)$$

Based on the theory of uniform elastic beam, the bending stiffness is proportional to the bending moment (Morse. 1936) by $M_x = -EI\frac{\partial^2 W}{\partial x^2}$. Therefore, with increasing lamina number for the fully bounded beams, the stiffness increases withN^3. On the other hand, for the frictionless case, the stiffness increases with N. These two cases match with previous research results (Pytel *et al*. 2011). To calculate the equivalent bending stiffness of a laminated beam using FEM it is possible to compare the results to those corresponding to an equivalent fully bounded one of the same overall height, the ratio is found to be

$$\frac{(EI)_b}{(EI)_{fullycoupled}} = \frac{(\zeta+1)^2N^3 - (\zeta^2+2\zeta)N}{N^3} \Rightarrow (EI)_b = (EI)_{fullycoupled}\frac{(\zeta+1)^2N^3 - (\zeta^2+2\zeta)N}{N^3} \quad (14)$$

where $(EI)_b$ is the stiffness of beam shown in Fig. 2(b).

2.2 Damping property

To calculate the loss factor of the system, the work done by friction and potential energy of bending is required. The friction between adjacent laminas, which is assumed to be a function of the relative slip distance, can be derived from the force equilibrium equation using the spring model, as shown in Eq. (15).

$$\int_{\varepsilon_l^i\frac{l}{\delta_I}}^{\varepsilon_u^i\frac{l}{\delta_I}} dF_x + F_{l,i-1} - F_{u,i} = \int_{\varepsilon_l^i\frac{l}{\delta_I}}^{\varepsilon_u^i\frac{l}{\delta_I}} dF_x + (k_{i-1}-k_i)\delta_E L_n = 0 \quad (15)$$

where the first term is the inner force caused by the lamina deformation. $F_{u,i}$ and $F_{l,i-1}$ are the force caused by the deformation of the spring-damping element, which equal to $F_{u,i} = k_i\varepsilon_u^i L_n$ and $F_{l,i-1} = k_{i-1}\varepsilon_l^{i-1}L_n$. It is also assumed that the free surfaces, i.e. the bottom and top surface, do not take any force such that $F_{l,0} = F_{u,N} = 0$. Therefore, the stiffness of the spring between i^{th} and i+1th can be expressed by Eq. (16).

$$k_i = \frac{\sum_{j=i}^{N} \int_{\varepsilon_l^j \frac{l}{\delta_I}}^{\varepsilon_u^j \frac{l}{\delta_I}} dF_x}{\delta_E L_n} = \frac{lEb\delta_I}{2\delta_E L_n}(\zeta+1)(N-i)i \tag{16}$$

The dissipation of energy, or work, is calculated by the friction force multiplied by the relative displacement between adjacent laminas, which is constant as mentioned above. Therefore, the dissipation energy is a function of N as shown in Eq. (17).

$$\begin{aligned} E_k &= \sum_{i=1}^{N} k_i L_n \delta_E L_n \delta_E \\ &= \sum_{i=1}^{N} \frac{lEb\delta_I}{2\delta_E L_n}(\zeta+1)(N-i)i(L_n\delta_E)^2 \\ &\propto N^3 - N \end{aligned} \tag{17}$$

On the other hand, as shown in Fig. 2, the deflection of the whole beam along the *x*-axis can be expressed as (Bournine *et al.* 2011)

$$w = W(1-\cos(\frac{\pi x}{2L_i})) \tag{18}$$

where W is the time-dependent deflection at the free end, which is approximately equal among all the laminas. Therefore, the potential energy due to bending is defined as the summation of the potential energy of all laminas.

$$\begin{aligned} E_b &= \sum_{i=1}^{N} \int_0^{L_i} \frac{1}{2}(EI)_i (\frac{\partial w^2}{\partial^2 x})^2 dx \\ &= \sum_{i=1}^{N} \frac{\pi^2 (EI)_i}{64 L_i}(W^2) \\ &\propto \sum_{i=1}^{N} \frac{\int_{\varepsilon_u^i \frac{l}{\delta_I}}^{\varepsilon_u^i \frac{l}{\delta_I}} dr^3}{\frac{(1+\varepsilon_u^i)L_n + (1+\varepsilon_l^i)L_n}{2}} \\ &\propto \sum_{i=1}^{N} \frac{\delta_I^2[(i-\frac{N}{2}) + \zeta(i-\frac{N+1}{2})]^3 - \delta_I^2[(i-\frac{N}{2}-1) + \zeta(i-\frac{N+1}{2})]^3}{1+\delta_I(i-\frac{N+1}{2})(1+\zeta)} \end{aligned} \tag{19}$$

Subsequently, the loss factor η can be expressed as a function of the lamination layers.

$$\eta = \frac{E_k}{E_b} \propto \frac{N^3 - N}{\sum_{i=1}^{N} \frac{\delta_I^2[(i-\frac{N}{2})+\zeta(i-\frac{N+1}{2})]^3 - \delta_I^2[(i-\frac{N}{2}-1)+\zeta(i-\frac{N+1}{2})]^3}{1+\delta_I(i-\frac{N+1}{2})(1+\zeta)}} \tag{20}$$

Hence, the loss factor can be obtained for given strain δ_I and strain difference ratio ζ. Using the equivalent parameters expressed in Eqs. (14) and (20), it is possible to predict the natural frequencies, as well as FRF of the beam.

3 Experimental and FEM Setup

The configuration of the experimental setup is shown in Fig. 4, and geometric and material parameters of a single Si-Fe sheet for the laminated beam are given in Table 1. The number of the laminas varied from 1 to 115. Laminas were held together by rubber bands at three locations along the beam's length to keep them tight.

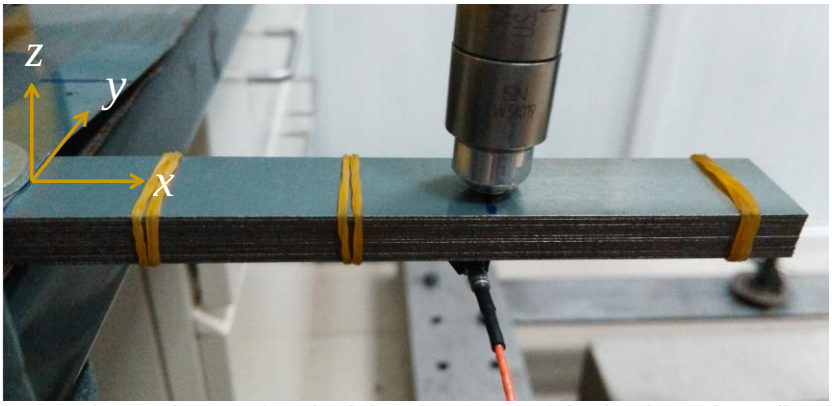

Figure 4: Experimental setup for obtaining the FRFs of the laminated cantilever beam

Table 1: Parameters of the Si-Fe sheets used for the laminated beam

Parameter	Value
Length, L_n *(m)*	0.12
Width, *b* (mm)	20
Thickness, *l* (mm)	0.5
Young's modulus, *E (GPa)*	133
Density, ρ *(kg/m³)*	7650
Poisson's ratio, *v*	0.28

The FRFs of the beam were measured using the impact force as the input and measuring the acceleration as the output. A PCB model 086C02 impact hammer was used to produce the impact force and a B&K 4517-002 accelerometer used to collect the response. Both locations of the impact force and accelerometer are 50 mm from the free end but one on the top and one at the bottom, as shown in Fig. 4. A National Instruments USB-6259 signal acquisition board with a LabVIEW interface program was used for data acquisition and signal processing.

To verify the analytical model, the experimental measured FRFs of laminated beams when N equals to 1, 8, 32 and 115 were used to optimise the parameters in Eqs. (14) and (20). These equations with fitted parameters were then used to estimate the stiffness and loss factors of the laminated beams with N equal to 2, 4, 16 and 64. FEM was used to calculate the FRF by using the equivalent bending stiffness and loss factor as input parameters.

It is recognised that for the real system it may be more likely that the changing physical parameter affecting the equivalent stiffness is the second moment of the area of the cross section. However, in the FEM simulation, when the solid beam configuration is used, this second moment of the area of the beam is equivalent to the solid beam. Therefore, the most efficient way to use equivalent bending stiffness is to use the equivalent Young's modulus.

4 Result and Discussion

4.1 Experimental result

Experimental measured FRFs up to 1000 Hz are shown in Fig. 5. The grey levels correspond to different numbers of the lamina. It is apparent in Fig. 5 that the loss factor rises with an increase in lamina number. The increase is caused by the greater potential for friction to do work between adjacent laminas. The natural frequencies slightly increase with the rise of lamina number, which is caused by the increase in thickness and the shear force from friction. However, this increase is much smaller compared to the fully bounded beam, according to Eq. (14).

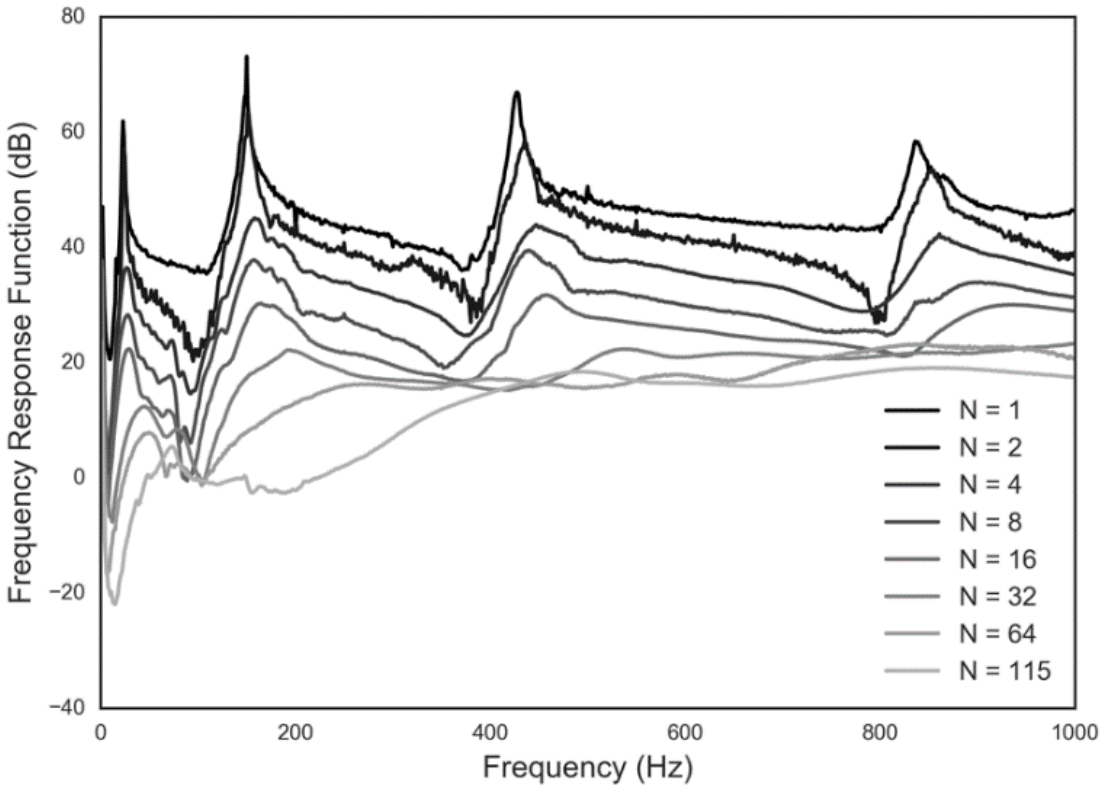

Figure 5: Measured FRFs of the laminated cantilever beam with different laminated layers

4.2 Parameters optimization and application

The loss factor and equivalent stiffness were calculated from the FRFs to be 0.025, 0.23, 0.38, 0.78 and 133, 2.1, 0.2, 0.08 GPa when N equaled 1, 8, 32 and 115, respectively. These two sets of parameters were used in FEM for subsequent FRF simulation and the predictions depicted in Fig. 6. The simulation result indicates the correctness by using equivalent material properties for modeling the vibration of the laminated cantilever beam.

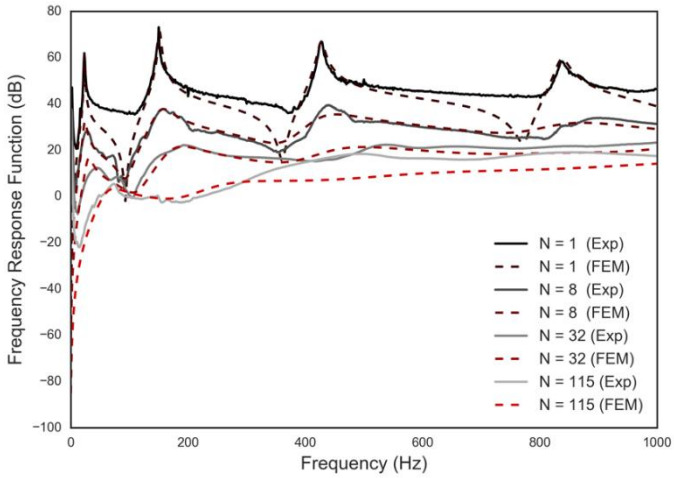

Figure 6: Experimental (solid lines) and FEM simulated (dash lines) FRFs of the cantilever laminated beams with lamina numbers $N = 1, 8, 32, 115$

By fitting Eqs. (14) and (20) with equivalent stiffnesses and loss factors, the equivalent stiffness and loss factor as functions of lamina number were obtained and the strain difference ratio ζ turns out to be -0.978, which subsequently produces the estimated loss factor under different layer numbers, as shown in Fig. 7(a) and (b). Recall that $\zeta = 0$ under the fully bonded case and $\zeta = -1$ under the frictionless case, the strain difference ratio $\zeta = -0.978$ in our experimental beam means the laminated bar with rubber band behaved similarly to the frictionless case. Small friction force and large slip displacement happened between adjacent laminas in our laminated beam. The calculated strain difference ratio is reasonable because most of the friction is introduced by the rough surface of the silicon steel sheet and rubber bands.

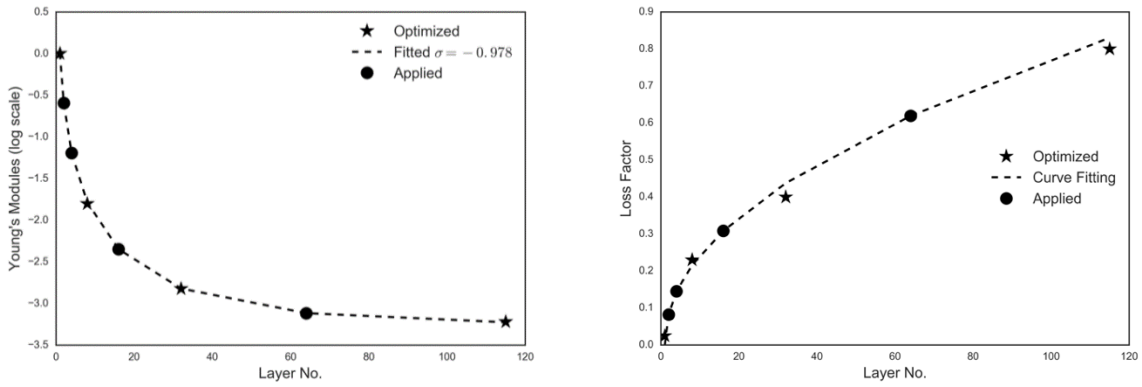

(a) (b)

Figure 7: (a) Equivalent Young's modulus in log scale ($N = 1$ as reference) and (b) loss factor versus lamina numbers with stars represent the samples used for parameters optimization, dash lines represent the fitted curve according to Eqs. (14) and (20), and dots represent the estimated equivalent Young's modulus and loss factor that is using for FEM simulation

The obtain of equivalent stiffnesses and loss factors are shown in both Fig. 7(a) and (b). Stars denote samples used for fitting of Eqs. (14) and (20) and dash lines are the fitted curve based on that. Then, the equivalent stiffnesses and loss factors to laminated beams with N equal to 2, 4, 16 and 64 were estimated from the fitted curves and applied to the FEM simulation.

Fig. 8 presents the simulated FRF via FEM based on estimated equivalent stiffness and loss factors. Results are compared between the simulated output (red dash) with experiment result (dark solid). It is apparent that both the natural frequencies and the loss factors present a close agreement.

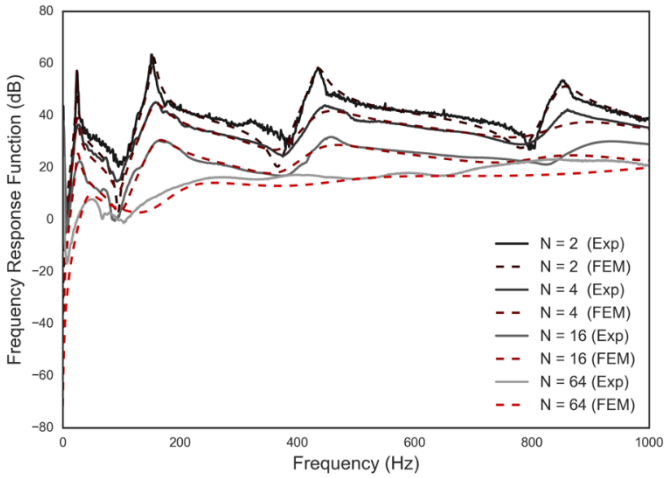

Figure 8: FRFs of different cantilever laminated beams simulated by equivalent stiffnesses and loss factors

5 CONCLUSIONS

To facilitate the calculation of frequency response functions for laminated structure by finite element method via equivalent material properties, a model was developed for calculating the equivalent bending stiffness and loss factors based on the relative strain and spring-damping model. The assumption is made that the whole beam performs a small deflection and the surface strain differences are constant within one lamina and between adjacent laminas. The internal strain difference and strain difference ratio are used as the key indicators to represent the friction and bonded condition between adjacent laminas. The equivalent stiffness is expressed as a function of lamina number and strains different ratio, which can be used for calculating the equivalent stiffness compare to the solid condition. The loss factor is calculated as the ratio between the dissipation of energy that is consumed by friction and the bending potential energy, which resolves to be as a function of lamina number and strain difference ratio. Finally, experimentally measured frequency response functions were obtained to calculate the strain difference ratio and other parameters when the lamina numbers were 1, 8, 32, and 115. The equivalent stiffnesses and loss factors when the lamina numbers were 2, 4, 16, and 64 were estimated based on the developed model and are used in the finite element method simulation. The finite element simulated frequency response function shows very close agreement with the experimental result, giving confidence to the model developed in this paper. In future, the strain difference ratio and other parameters will be obtained on a real transformer and the frequency response functions on the transformer core will be simulated and compared.

ACKNOWLEDGEMENTS

The financial support from the Australia Research Training Scholarship, NSFC (Grant No. 11574269), and Jiewei Du, who provided the experimental data, are gratefully acknowledged.

REFERENCES

Girgis, Ramsis, Jan Anger, and Donald Chu. 2008. 'The sound of silence'. *ABB review* 2: 47-51.

Wang, Yuxing, Jie Pan, and Ming Jin. 2011. 'Finite element modelling of the vibration of a power transformer'. *Proc. Acoustics*. Fremantle, Australia.

Pirnat, Miha, Gregor Čepon, and Miha Boltežar. 2013. 'Introduction of the linear contact model in the dynamic model of laminated structure dynamics: an experimental and numerical identification'. *Mechanism and Machine Theory* 64: 144-154.

Du, Jiewei, et al. 2017. 'Vibration characteristics of transformer core components'. *INTER-NOISE and NOISE-CON Congress and Conference Proceedings*. 255 (3): 4531-4540.

Bournine, Hadjila, David J. Wagg, and Simon A. Neild. 2011. 'Vibration damping in bolted friction beam-columns'. *Journal of Sound and Vibration* 330(8): 1665-1679.

Pytel, Andrew, and Jaan Kiusalaas. 2011. *Mechanics of Materials*. 2nd ed. Boston: CengageLearning

Morse, P. M. 1936. 'Vibration and sound (Vol. 3)'. New York: McGraw-Hill.